Dark field sensitivity in single mask edge illumination lung imaging

DARK FIELD SENSITIVITY IN SINGLE MASK EDGE ILLUMINATION LUNG IMAGING

Jonathan Sanctorum, Jan Sijbers, Jan De Beenhouwer

imec-Vision Lab, Department of Physics, University of Antwerp,
Universiteitsplein 1, 2610 Antwerp, Belgium

ABSTRACT

X-ray phase contrast imaging is a rapidly evolving field, covering a range of different imaging methods. Its integration in the daily medical imaging routines, however, has proven to be difficult, despite encouraging results. In addition to the phase information, small angle X-ray scattering information is accessible through the so called dark field signal. The dark field signal holds great potential for lung imaging applications due to its ability to detect sub-pixel structures. Edge illumination, an incoherent form of phase contrast imaging, is particularly promising due to its low coherence requirements. A remaining issue in conventional edge illumination phase contrast imaging, however, is the absorption of photons by the detector mask, as these photons contribute to the dose but not to the image. In this work, we explore the dark field potential of a setup without detector mask for lung imaging through Monte Carlo simulations. In order to approximate the irregular shape of alveoli, surface roughness is taken into account.

***Index Terms*—** X-ray phase contrast imaging, dark field imaging, edge illumination, computer simulation, lung

1. INTRODUCTION

Conventional, attenuation based X-ray imaging has been embraced by the medical community since its discovery and has, among other applications, become the standard method for the inspection of bone fractures [1]. Whereas attenuation based X-ray imaging is very successful in distinguishing bone from soft tissue, discrimination between different types of soft tissue based on attenuation contrast can be a challenging task. X-ray phase contrast imaging (XPCI), on the other hand, is well-suited for this purpose [2], as it does not rely on attenuation differences but on the local refraction of X-rays.

Several practical implementations of XPCI exist, and these can be roughly divided into two classes: interferometric methods and non-interferometric methods. This work focuses on edge illumination (EI)[3], which is a non-interferometric method. In addition to the phase contrast image, EI also yields the conventional attenuation image and the so-called dark field image. The latter is a measure for the amount of small angle scattering within the sample, originating from sub-pixel structures that cannot be resolved directly with the detector [4]. From the perspective of (potential) medical applications, the human lungs are of great interest, as they exhibit a complex microstructure consisting out of hundreds of millions of pulmonary alveoli [5].

As will be explained in Section 2, the conventional EI setup involves placing an absorption grating in front of the detector, partially masking the detector pixels. This configuration blocks a significant amount of the photons arriving at the detector, after interaction with the imaged object. This has a negative effect on the delivered dose, but is in principle resolved by removing the detector mask.

In this work we will, through Monte Carlo simulations, explore the potential of dark field imaging with an EI setup without detector mask, also known as single mask EI [6] or beam tracking [7], depending on the exact implementation. More specifically, we will quantify the relative broadening of the X-ray beam due to small angle scattering. In order to approximate the irregular shape of pulmonary alveoli [8], surface roughness is taken into account in our digital phantom and its influence on the beam broadening is evaluated.

2. METHODS

2.1. Edge illumination

A conventional EI setup consists out of an X-ray source and detector, with two parallel gratings or masks placed in between. This is shown in Fig. 1. During an EI acquisition, the sample is placed directly behind the sample mask for imaging.

The first mask, which we will refer to as the sample mask, acts as a beam splitter, dividing the incoming X-ray beam into several smaller beamlets. The position of the sample mask can be chosen such that these beamlets hit the edges of the second mask, referred to as the detector mask. The detector mask coincides with the pixel edges, leaving only the central part of each pixel exposed to incoming radiation. In this configuration, a deflection of a certain beamlet will either increase or decrease the intensity measured in the corresponding pixel. As such, refraction of the beamlets can be detected, effectively making the system sensitive to phase variations.

In order to retrieve all three signals (phase, attenuation and dark field), the sample mask is shifted perpendicular to

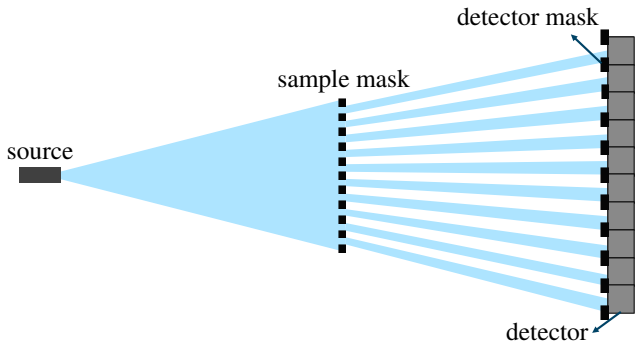

Fig. 1. Schematic overview of a conventional two mask edge illumination setup (not to scale).

the grating bars, hereby changing the amount or radiation incident on the detector pixels [3]. Gradually shifting the beamlet over one period of the detector mask generates a Gaussian intensity modulation in each pixel, called the illumination curve (IC). In practice, the IC is sampled for a small set of sample mask positions and a Gaussian fitting procedure is performed. The three signals are subsequently retrieved from the fitting parameters.

As can be seen from Fig. 1, both the sample mask and detector mask block arriving photons, resulting in a significant loss of photons. In the context of medical imaging, the loss of photons at the sample mask is less important, as this does not affect the patient dose. A straightforward approach to avoid the loss of photons at the detector mask or reduce acquisition time (single shot), is to simply remove the mask from the EI setup, which is shown in Fig. 2. This, however, drastically changes the geometry, raising the question to which extent we are still able to retrieve the signals of interest.

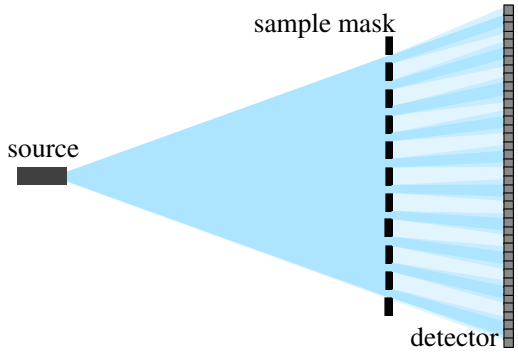

Fig. 2. The considered single mask edge illumination setup (not to scale).

Given its relevance to lung imaging [5], we will investigate the sensitivity of such an adjusted system for dark field imaging by quantifying the beam broadening directly from simulated beamlet intensity profiles.

To this end, we consider a geometry with three adjacent beamlets, as shown in Fig. 3, configured to illuminate 12 pixels in total. As opposed to conventional EI, each beamlet covers more than one detector pixel. Assuming a Gaussian focal spot, the beamlet intensity profiles exhibit Gaussian shapes as well.

The broadening is measured by determining the standard deviation of the Gaussian fitted to the central beamlet and comparing this to the standard deviation of the unaltered beamlet without object in the beam.

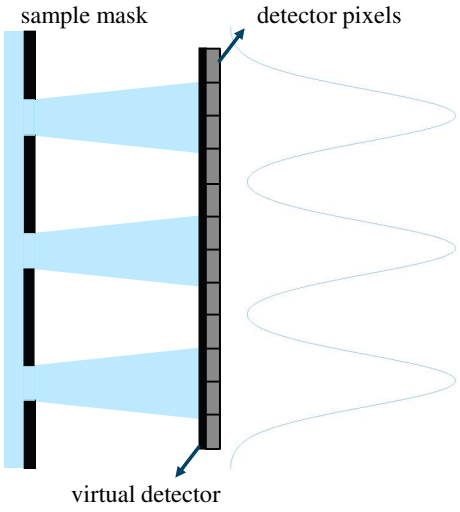

Fig. 3. Schematic view of the three beamlets considered in the simulations (not to scale). The corresponding Gaussian intensity profile at the detector is shown as well.

2.2. Simulation framework

The simulations are performed using an extended version of GATE [9], an application layer on top of the Geant4 Monte Carlo software [10]. The extensions on the physics side, assigning a phase to each photon and incorporating Snell's law for refraction, allow the simulation of XPCI using GATE. The full framework was originally implemented for grating based phase contrast imaging, an interferometric method, and thus includes a subsequent numerical wavefront propagation part to account for interference effects. EI, however, is inherently non-interferometric, meaning this wavefront propagation part can be omitted. As a consequence, the full experimental flow is modeled in GATE, from photon generation at the source to detection.

In order to simultaneously monitor pixel measurement and beamlet intensity profiles, a virtual detection plane is inserted in front of the actual detector (Fig. 3), acting as a virtual high resolution photon counting detector with 100% detection efficiency. This virtual plane is, however, transparent to the photons and does not influence the pixel measurements.

2.3. Surface roughness

In GATE, test phantoms can easily be defined using geometrical building blocks such as boxes and spheres. As these are continuous in space, voxelization effects do not hamper the refraction. Indeed, a determining factor in the X-ray refraction process, which is called when a photon crosses the boundary between two materials, is the orientation of the surface normal. Pulmonary alveoli are highly irregular in shape [8], but the geometrical building blocks in GATE, on the other hand, exhibit perfectly smooth surfaces. To account for this, we have introduced a simple yet effective surface roughness model for X-rays in GATE [9]. In this model, a random process is triggered whenever a photon crosses a material boundary, locally changing the orientation of the surface normal. The direction of this change is drawn uniformly, while its magnitude follows a Gaussian distribution centered around 0. As the amount of variation introduced in the simulation is determined by the standard deviation of the Gaussian distribution, we will use this parameter as a measure for the surface roughness of the phantom.

3. EXPERIMENTS

Since dark field imaging of lungs is of key interest, the phantom designed for our simulations exhibits a strong microstructure. It is designed as a collection of hollow glass spheres with radius 23 μm, randomly distributed in water, and accounting for approximately 30% of the total phantom volume. The hollow spheres are filled with air, and in total the phantom measures 10 cm in thickness. This phantom is placed directly behind the sample mask in GATE, which in turn is positioned 1875 mm downstream of the source. The total distance between source and detector is 2500 mm, resulting in a geometrical magnification factor of 4/3. The sample mask is made of 300 μm Tungsten and has a period of 450 μm, with an aperture of 150 μm forming the beamlets. In our simulated setup, no detector mask is present. The CsI detector measures 550 μm in thickness, consists out of pixels with a size of 150 μm and is preceded by both a 250 μm plastic layer and a 750 μm carbon layer. During each simulation, $30{\cdot}10^6$ photons are emitted from a polychromatic (60 kVp, 1.1 mm Al filtration) source in a fan beam geometry. The focal spot is Gaussian in shape with a FWHM of 600 μm, in line with clinical conditions.

In order to investigate the effect of the surface roughness of the phantom, the simulation is repeated for 7 different roughness levels, defined through the standard deviation of the Gaussian distribution: $0°$, $3°$, $6°$, $9°$, $12°$, $15°$ and finally $18°$. As mentioned in Section 2.2, a virtual detector is placed in front of the actual detector pixels in order to simultaneously extract the pixel measurements and beamlet profiles. The latter are sampled at 1 μm and subsequently used to quantify the beamlet broadening.

4. RESULTS AND DISCUSSION

Simulated beamlet intensity profiles are shown in Fig. 4. For clarity of the plot, the results for $3°$, $9°$, and $15°$ are omitted. As can be seen from this figure, increasing the surface roughness lowers the intensity modulation in the beamlet profiles, indicating an increased beamlet broadening.

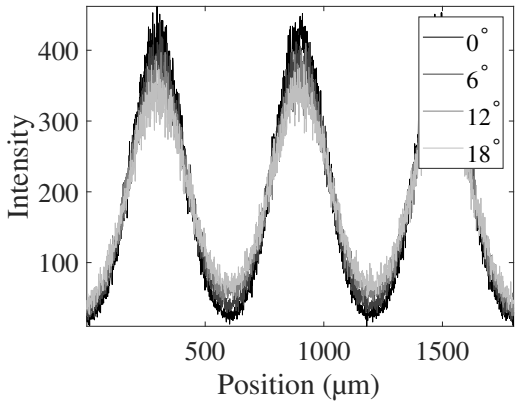

Fig. 4. Simulated beamlet profiles for surface roughness values of $0°$, $6°$, $12°$ and $18°$.

The broadening was subsequently quantified for every considered roughness value, by determining the standard deviation of a Gaussian fitted to the beamlets and comparing this to the standard deviation in the absence of a phantom as a reference. This resulted in the relative width increase of the beamlets (the broadening), which is plotted in Fig. 5.

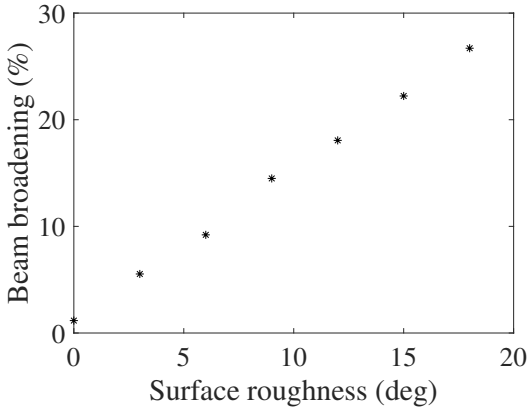

Fig. 5. Relative beamlet broadening calculated from the beamlet profiles shown in Fig. 4.

The plot confirms the previous observation based on Fig. 4 that an increased surface roughness results in stronger beam broadening. Furthermore, this increase appears to behave linearly.

To give an indication of the dark field sensitivity of the

simulated setup, the question raises whether or not this increase in beam broadening translates into a measurable change in pixel intensity at the detector. The detector pixel measurements corresponding to the beamlet profiles in Fig. 4 are plotted in Fig. 6. As can be seen from this plot, the changes in beam broadening indeed affect the intensity measured in the pixels. The latter is an encouraging result in the context of lung imaging using EI, as this indicates that a single mask setup indeed has the potential to achieve sufficient dark field sensitivity.

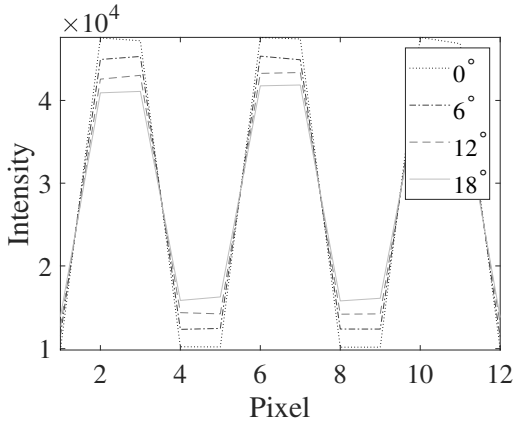

Fig. 6. Simulated detector pixel measurements for surface roughness values of 0°, 6°, 12° and 18°.

5. CONCLUSION

In this work, we have explored the potential of a single mask EI setup for dark field imaging using numerical simulations in GATE. It was shown that increasing surface roughness affects the broadening of the beamlets. Furthermore, this variation was visible in the simulated pixel measurements. This is a strongly encouraging result in the search for practical lung imaging solutions based on EI dark field contrast imaging. Here, simulated high resolution beamlet profiles were used to quantify the broadening. In practical applications however, the broadening (and thus the dark field) can only be measured from the pixel values and suitable methods are currently under development. The parameter range explored in this work was chosen mostly for demonstration purposes. Determination of representative roughness values based on experimental measurements is work in progress. Finally, future experiments will shed light on the trade-off between faster imaging and expected loss of resolution compared to conventional EI setups.

6. COMPLIANCE WITH ETHICAL STANDARDS

This is a numerical simulation study for which no ethical approval was required.

7. ACKNOWLEDGMENTS

This research was supported by EU Interreg Flanders - Netherlands Smart*Light (0386), Research Foundation - Flanders (FWO) (G090020N, G094320N), and Agentschap Innoveren & Ondernemen (Vlaio) (HBC.2020.2159).

8. REFERENCES

[1] Gordian Lukas Schmid et al., "The Investigation of Suspected Fracture - a Comparison of Ultrasound With Conventional Imaging," *Deutsches Ärzteblatt International*, vol. 114, no. 45, pp. 757–764, Nov. 2017.

[2] Marco Endrizzi, "X-ray phase-contrast imaging," *Nuclear Instruments & Methods in Physics Research A*, vol. 878, pp. 88–98, Jan. 2018.

[3] Marco Endrizzi and Alessandro. Olivo, "Absorption, refraction and scattering retrieval with an edge-illumination-based imaging setup," *Journal of Physics D: Applied Physics*, vol. 47, pp. 505102, Nov. 2014.

[4] Wataru Yashiro et al., "On the origin of visibility contrast in x-ray Talbot interferometry," *Optics Express*, vol. 18, no. 16, pp. 16890, Aug. 2010.

[5] Konstantin Willer et al., "X-ray dark-field imaging of the human lung—A feasibility study on a deceased body," *PLOS ONE*, vol. 13, no. 9, pp. e0204565, Sep. 2018.

[6] Gibril K. Kallon et al., "Comparing signal intensity and refraction sensitivity of double and single mask edge illumination lab-based x-ray phase contrast imaging setups," *Journal of Physics D: Applied Physics*, vol. 50, no. 41, pp. 415401, Oct. 2017.

[7] Fabio A. Vittoria et al., "Beam tracking approach for single–shot retrieval of absorption, refraction, and dark–field signals with laboratory x–ray sources," *Applied Physics Letters*, vol. 106, no. 22, pp. 224102, Jun. 2015.

[8] Alison A. Hislop, Jonathan S. Wigglesworth, and Ritti Desai, "Alveolar development in the human fetus and infant," *Early Human Development*, vol. 13, no. 1, pp. 1–11, Feb. 1986.

[9] Jonathan Sanctorum, Jan De Beenhouwer, and Jan Sijbers, "X-ray phase contrast simulation for grating-based interferometry using GATE," *Optics Express*, vol. 28, no. 22, pp. 33390–33412, Oct. 2020.

[10] Giovanni Santin et al., "GATE: A Geant4-based simulation platform for PET and SPECT integrating movement and time management," *IEEE Transactions on Nuclear Science*, vol. 50, no. 5, pp. 1516–1521, Oct. 2003.